Detailed 3D modelling of mass transfer processes in two phase flows with dynamic interfaces

D. Darmana, N.G. Deen*, J.A.M. Kuipers

Fundamentals of Chemical Reaction Engineering, Faculty of Science and Technology, University of Twente, P.O. Box 217, 7500 AE Enschede, The Netherlands

Abstract

We developed a method that will enable us to determine mass transfer coefficients for a large number of two phase flow conditions based on numerical simulation. A three-dimensional direct numerical simulation based on the Front Tracking technique taking into account the mass transfer process was chosen for this purpose. The dissolved species concentration in the liquid phase is tracked using a scalar mass balance while the value of the concentration at the interface is determined via an immersed boundary technique. In the present study, simulations are carried out to investigate the effect of the bubble shape on the dissolved species concentration field.

1 Introduction

Gas-liquid chemical reactors have been studied extensively, both experimentally and numerically. However, because of the complex hydrodynamics, mass transfer and chemical reaction as well as their interaction, there is still a lack of fundamental understanding of their dynamics.
With recent advances in computer power, it becomes computationally feasible to simulate a three dimensional gas-liquid chemical reactor using Euler-Euler or Euler-Lagrange models. Using either one of the models, large scale hydrodynamics, mass transfer and chemical reaction can be revealed. However, as both models require a set of closures to specifically describe a particular system, the reliability of the results strongly depends on the accuracy of the provided closure.
Traditionally the closure is obtained via experimental measurements in well controlled systems. Only recently scientists try to obtaine the closure purely based on numerical simulations. As an example, using front tracking and volume of fluid model, Dijkhuizen et al. [1] tried to extract hydrodynamics (drag, lift and virtual mass) closure and found good agreement with experimental data reported in the literature. Furthermore, based on two dimensional front tracking modelling with additional mass balance equations, Koynov et al. [2] shows that the mass transfer coefficient can also be extracted from numerical simulation of an isolated bubble.
From experimental data published by Grace [3] it is known that the physical properties of a gas-liquid systems will determined the bubble shape as well as its rise velocity. These parameters, in turn affect the hydrodynamics of the flow around the bubbles and consequently the gas-liquid mass-transfer and the liquid-phase transport. It has become evident that in order to accurately predict the mass transfer coefficient a model should be able to render correctly the shape of the bubble as well as the rise velocity for a given set of physical properties.
A three dimensional Front Tracking code (FT3D) has been developed in our group. Using FT3D, Van Sint Annaland et al. [4] conducted numerical tests to verify the correctness of the hydrodynamics part of the model. The authors shown that the model can predict various bubble shapes as

* *Email address:* N.G.Deen@tnw.utwente.nl

well as its rise velocity indicated in the Grace diagram. In the present study, FT3D is extended by adding species transport equations to allow simulation with mass transfer and chemical reaction. The code is used to investigate the effect of the bubble shape to the transport of the dissolved species. The ultimate goal of this study will be that using the developed model we are able to accurately predict all of the closures required to simulate a gas-liquid chemical reactor using large scale models such as the Euler-Euler model or the Euler-Lagrange model.

2 Governing equations

For incompressible two phase flows the Navier-Stokes equations describing the fluid flow is described as:

$$\nabla \cdot \rho \mathbf{u} = 0 \tag{1}$$

$$\frac{\partial \rho \mathbf{u}}{\partial t} + \nabla \cdot \rho \mathbf{u}\mathbf{u} = -\nabla p + \rho \mathbf{g} + \nabla \cdot \mu \left[(\nabla \mathbf{u}) + (\nabla \mathbf{u})^T \right] + \mathbf{F}_\sigma \tag{2}$$

where $\mathbf{F}_\sigma$ is the local volumetric surface force accounting for the presence of the disperse phase. The local averaged density ρ and viscosity μ are evaluated from the local distribution of the phase indicator or colour function F which is governed by a Poisson equation given as :

$$\nabla^2 F = \nabla \cdot \mathbf{G} \tag{3}$$

where the vector quantity $\mathbf{G}$ contains the information of the spatial distribution of the interface. For the local average density ρ linear weighing of the density of the continuous (ℓ) and disperse phase (g) is used :

$$\rho = F\rho_\ell + (1 - F)\rho_g \tag{4}$$

The local average viscosity is calculated via harmonic averaging of the kinematic viscosities of the involved phases following a recent approach proposed by Prosperetti [5] :

$$\frac{\rho}{\mu} = F\frac{\rho_\ell}{\mu_\ell} + (1 - F)\frac{\rho_g}{\mu_g} \tag{5}$$

The mass-balance equations for a chemical species dissolved in the liquid, Y_i, can be written as:

$$\frac{\partial}{\partial t}(\rho Y_i) + \mathbf{u} \cdot \nabla (\rho Y_i) - D_i \nabla^2 (\rho Y_i) = q \tag{6}$$

where q is a volumetric forcing term, which will ensure that the value of the species at the interfacial is equal to the value prescribed by Henry's law.
Here

$$\rho Y_i (x, y, z, t) = \rho_\ell Y_{\ell,i} F + \rho_g Y_{g,i} [1 - F] \tag{7}$$

where $Y_{\ell,i}$ is the mass fraction of species i in the liquid phase and $Y_{g,i}$ is its mass fraction in the gas phase;

3 Numerical solution method

Flow field

In order to handle systems with very large density ratios, the Navier-Stokes equations are rewritten in the non-conservative form using the continuity equations:

$$\rho \left[\frac{\partial \mathbf{u}}{\partial t} + (\nabla \cdot \mathbf{u}\mathbf{u}) \right] = -\nabla p + \rho \mathbf{g} + \nabla \cdot \mu \left[(\nabla \mathbf{u}) + (\nabla \mathbf{u})^T \right] + \mathbf{F}_\sigma \tag{8}$$

where the density on the left hand side is evaluated at the old time level. The non-conservative form of the Navier-Stokes equations is solved with a standard finite difference technique on a staggered rectangular three-dimensional grid using a two-step projection-correction method with an implicit treatment of the pressure gradient and explicit treatment of the convection and diffusion terms. A second order flux delimited Barton-scheme is used for the discretization of the convective terms and standard second order central finite difference for the diffusion terms. The resulting Pressure Poisson Equation (PPE) is solved using the Conjugate Gradient method with the Block Jacobi method selected as preconditioner.

Interface tracking and phase indicator

The corner points of the surface elements (markers) are moved with an interpolated velocity field using a first order Euler method:

$$\mathbf{r}^{n+1} = \mathbf{r}^n + \mathbf{u}^{n+1}\Delta t \tag{9}$$

where $\mathbf{r}^n$ and $\mathbf{r}^{n+1}$ indicate respectively the old (time level n) and new (time level $n+1$) position vectors, whereas $\mathbf{u}_m^{n+1}$ represents the interpolated velocity field at the new time level.
The spatial distribution of the phase indicator F is solved by first calculating the spatial interface vectors $\mathbf{G}$ using the method proposed by Unverdi and Tryggvason [6]:

$$\mathbf{G} = \sum_m D\left(\mathbf{x} - \mathbf{x}_m\right)\mathbf{n}_m \Delta s_m \tag{10}$$

Using $\mathbf{G}$ given by Eq. 10, the Poisson-equation for the colour function F (Eq. 3) is discretized using standard finite difference method. The resulting set of linear equations is solved using the Incomplete Cholesky Conjugate Gradient (ICCG) algorithm.

Surface force

The net surface force acting on a single surface element m is calculates as:

$$\mathbf{F}_{m,s} = \oint \sigma\left(\mathbf{t} \times \mathbf{n}\right) \tag{11}$$

where $\mathbf{t}$ is the tangent vector (or edge) shared by element m and $\mathbf{n}$ is the unit normal vector.
In the discrete form, Eq. 11 is written as:

$$\mathbf{F}_{m,s} = \sum_k \sigma\left(\mathbf{t}_k \times \mathbf{n}_k\right) \tag{12}$$

where k represents the neighboring elements of the element m. The tangent vectors is directly calculated form the known positions of the three corner points of the element. The volumetric surface force in the Eulerian grid is obtained by mapping individual net surface force from all elements:

$$\mathbf{F}_\sigma\left(\mathbf{x}\right) = \frac{\sum_m \sum_k \rho_{m,k} D\left(\mathbf{x} - \mathbf{x}_{m,k}\right)\sigma\left(\mathbf{t}_{m,k} \times \mathbf{n}_{m,k}\right)}{\sum_m \sum_k \rho_{m,k} D\left(\mathbf{x} - \mathbf{x}_{m,k}\right)} \tag{13}$$

here, additional density weighing is used to avoid distribution of the surface force to cells that have a very low liquid volume fraction.

Mass transfer

For the species balance given in Eq. 6, a standard central scheme is applied to the diffusive term while an upwind scheme is used to discretize the convective term. Furthermore, a first order Euler scheme is used to discretized the temporal term. For every chemical species involved in

the system (including the background liquid) a species balance equations is used. The resulting discretized equations for all species are solved simultaneously using an algorithm similar to that used by Hjertager [7] in solving the mass conservation equations in a multi-fluid model and has been also used by Darmana et al. [8] for solving chemical species balance in a discrete bubble model simulation employing mass transfer and chemical reaction.
The value of the concentration at the interfaces is imposed using an immersed boundary technique following the work of Uhlmann [9]. In this technique a volumetric forcing term q is determined in such way that the resulting solution of eq. 6 gives a proper value of the concentration at the interfaces in an interpolated manner. The q term is determined by first calculating the forcing term Q_m for each individual marker m:

$$Q_m = \frac{(\rho Y)_m^d - (\rho Y)_m^{n+1}}{\Delta t} \tag{14}$$

where $(\rho Y)_m^d$ and $(\rho Y)_m^{n+1}$ respectively are the desired concentration and the interpolated concentration value at the marker position. $(\rho Y)^{n+1}$ is obtained by solving eq. 6 with $q = 0$. Given forcing at Lagrangian marker Q_m, the volumetric forcing term is calculated by mapping all of the Lagrangian forcing terms to the Eulerian grid:

$$q(\mathbf{x}) = \sum_m D\left(\mathbf{x} - \mathbf{x}_m\right) \frac{Q_m \Delta V_m}{V_{cell}} \tag{15}$$

where ΔV_m is the volume associated with marker m defined as $V_m = A_m (V_{cell})^{1/3}$, A_m is the area of marker m and V_{cell} is the volume of computational cell $V_{cell} = dx \cdot dy \cdot dz$.

4 Results

In the present study, transport of dissolved chemical species originally residing in the gas bubbles is demonstrated as a function of bubble shape. Two simulations using parameters which are represented by dimensionless Morton ($\mathrm{Mo} = \frac{g\mu_\ell^4 \Delta\rho}{\rho_\ell^3 \sigma^3}$), Eötvös ($\mathrm{Eo} = \frac{g\Delta\rho d_e^2}{\sigma}$) , Reynolds ($\mathrm{Re} = \frac{\rho_\ell v_\infty d_e}{\mu_\ell}$) and Schmidt ($\mathrm{Sc}_i = \frac{\mu_\ell}{\rho_\ell D_i}$) numbers are used. Here d_e is defined as the diameter of a spherical bubble with the same volume as the bubble under consideration, moreover v_∞ represents the terminal rise velocity of the bubble.
Fig. 1 shows the initial bubble shape and position. Computational grids used for the simulation are $50 \times 50 \times 100$ and a time step of $1 \times 10^{-4} s$. Twenty (20) computational grid cells used inside the bubble at its initial shape. A fixed density and viscosity ratio of one hundred was used. This density and viscosity ratio is believed to be high enough to mimic gas-liquid systems with sufficient accuracy. To reduce the number of required computational grid cells, a window shifting technique is used to maintain bubbles at its original position.

Figure 2 and 3 show series of snapshots of the bubble shape, velocity field and the normalized dissolved species concentration at different times. As we can see bubbles which originally have a spherical shape gradually evolve into two different shapes because of differences in the physical properties. In case 1, an intermediate ellipsoidal and wobbling bubble is obtained while in case 2 an intermediate skirted and ellipsoidal bubble is produced. In table 1 the values of the selected Morton and Eötvos numbers are given. In this table Re_G and Re_C represent respectively the bubble Reynolds number obtained from the Grace diagram and the computed bubble Reynolds number. It can be seen that for the two cases, the computed Reynolds number and bubble shapes compare very well with the data obtained from the Grace diagram.
With different bubble shape, the hydrodynamics surrounding the bubble also differ which in turns gives different transport characteristics for the dissolved gas near the bubbles surface. The concentration field clearly shows this behavior. In case 1, the bubble has a single wake at the center

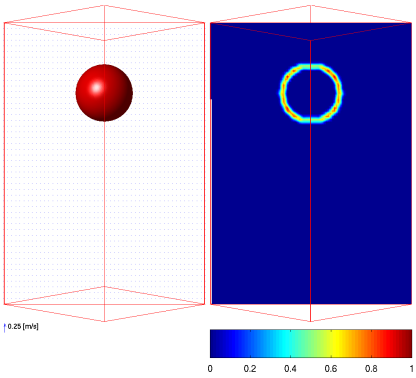

Figure 1: Initial conditions use in the simulation

Table 1: Morton (Mo), Eötvos (Eo) and Schmidt (Sc) numbers for the two cases. Re_G and Re_C represent respectively the bubble Reynolds number obtained from the Grace diagram and the computed bubble Reynolds number.

Case	Bubble regime	M	Eo	Sc	Re_G	Re_C
1	Intermediate ellipsoidal and Wobbling	5×10^{-7}	3.125	300	100	90
2	Intermediate skirted and ellipsoidal	9.2×10^{-3}	40	300	30	28.4

bottom region of the bubble. The dissolved gas is contained exclusively in the bubble wake. In case 2 however, the bubble wake is generated at the edge of the skirted bubble. The high concentration of dissolved gas that is trapped below the bubble is flowing through this edge generating a tubular region rich with dissolved gas while the middle region has a relatively low concentration of the dissolved gas.
Already from this two simulations we have a solid evidence that the bubble shape influences the mass transfer process, however more quantitative comparison by actually measuring the amount of gas being transfered to the liquid phase still needs to be done.

5 Conclusion

In this paper a three-dimensional Front Tracking model taking into account mass transfer calculated with an immersed boundary technique has been presented. Simulations with two different physical properties have been conducted to demonstrate the capabilities of the model. The computed terminal Reynolds numbers and shapes of the bubbles rising in quiescent liquids are compared with data taken from the bubble diagram of Grace. It was demonstrated that the computed shapes and rise velocity agree very well with the data taken from this diagram. It is also found that different bubble shapes lead to different hydrodynamics surrounding the bubble, which influences the transport of the dissolved gas in the liquid. In the near future, the mass transfer coefficient will be neasured numerically and the influence of the bubble shape to the coefficient will be investigated.

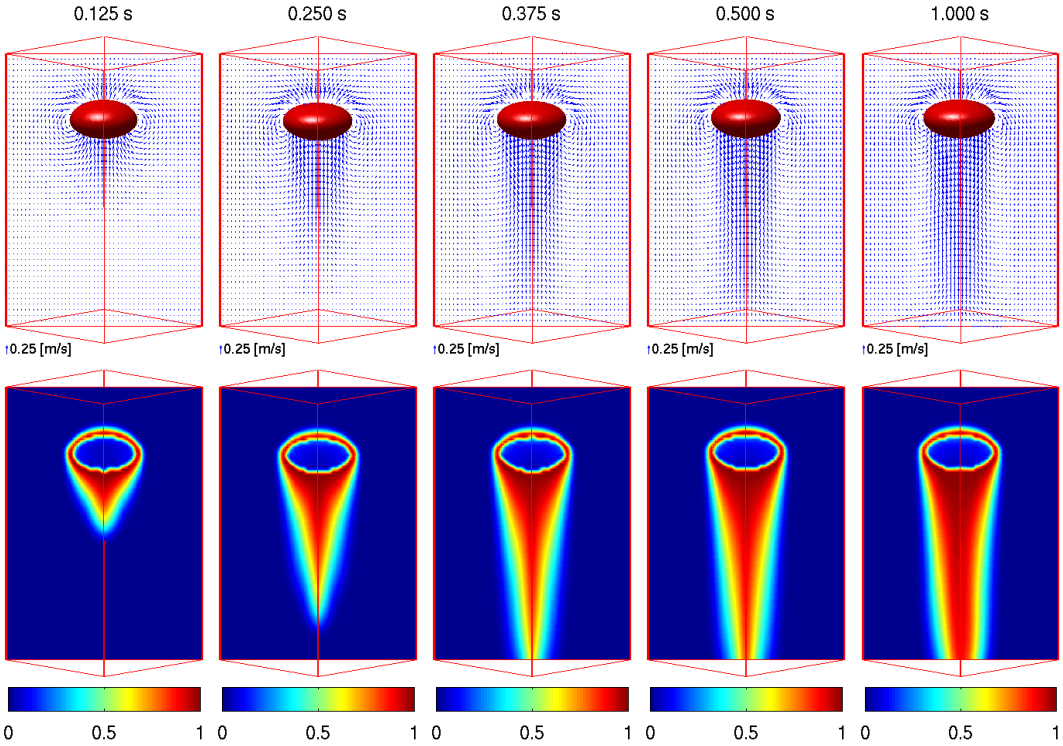

Figure 2: Case 1: Intermediate ellipsoidal and Wobbling, M $= 5 \times 10^{-7}$, Eo $= 3.125$, Sc $= 300$. Bubble shape and velocity vector (top); Normalized dissolved species concentration (bottom).

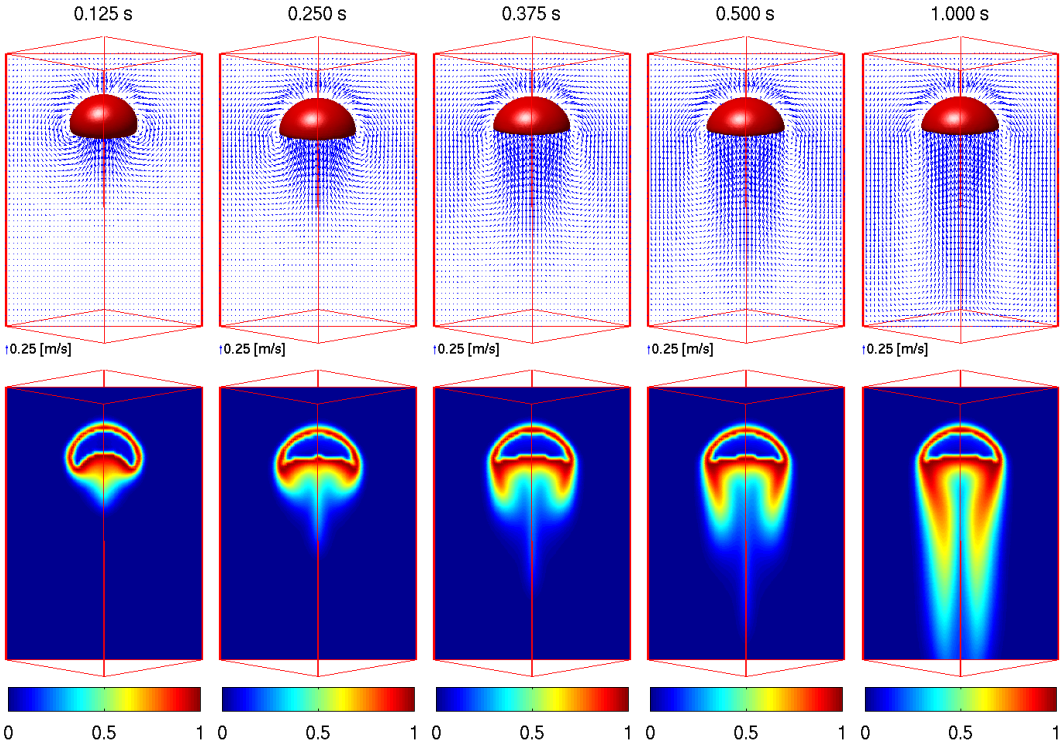

Figure 3: Case 2: Intermediate skirted and ellipsoidal, M $= 9.2 \times 10^{-3}$, Eo $= 40$, Sc $= 300$. Bubble shape and velocity vector (top); Normalized dissolved species concentration (bottom).

References

[1] W. Dijkhuizen, E. I. V. van den Hengel, N. G. Deen, M. van Sint Annaland, J. A. M. Kuipers, Numerical investigation of closures for interface forces acting on single air-bubbles inwater usingvolume of fluid and front tracking models, Chemical Engineering Science 60 (2005) 6169–6175.

[2] A. Koynov, J. G. Khinast, G. Tryggvason, Mass transfer and chemical reactions in bubble swarms with dynamic interfaces, AIChE Journal 51 (10) (2005) 2786–2800.

[3] J. R. Grace, Shapes and velocities of bubbles rising in infinite liquids, Trans. Instn. Chem. Eng 51 (1973) 116–120.

[4] M. van Sint Annaland, W. Dijkhuizen, N. G. Deen, J. A. M. Kuipers, Numerical simulation of gas bubbles behaviour using a 3D front tracking method, AIChE Journal 52 (2006) 99–110.

[5] A. Prosperetti, Drop-surface interaction, Wien: Springer, 2002, Ch. A Navier-Stokes numerical algorithms for free-surface flow computations: An overview, pp. 237–257.

[6] S. O. Unverdi, G. A. Tryggvason, A front-tracking method for viscous, incompressible multi-fluid flows, J. Comp. Phys 100 (1992) 25–37.

[7] B. H. Hjertager, Computational fluid dynamics (CFD) analysis of multiphase chemical reactors, Trends in Chemical Engineering 4 (1998) 44–92.

[8] D. Darmana, N. G. Deen, J. A. M. Kuipers, Detailed modeling of hydrodynamics, mass transfer and chemical reactions in a bubble column using a discrete bubble model, Chemical Engineering Science 60 (2005) 3383–3404.

[9] M. Uhlmann, An immersed boundary method with direct forcing for the simulation of particulate flows, Journal of Computational Physics 209 (2005) 448–476.